Hyperammonemia in gene-targeted mice lacking functional hepatic glutamine synthetase

Natalia Qvartskhava[a,1], Philipp A. Lang[a,b,1], Boris Görg[a], Vitaly I. Pozdeev[a], Marina Pascual Ortiz[a], Karl S. Lang[c], Hans J. Bidmon[d], Elisabeth Lang[a], Christina B. Leibrock[e], Diran Herebian[f], Johannes G. Bode[a], Florian Lang[e], and Dieter Häussinger[a,2]

[a]Department of Gastroenterology, Hepatology, and Infectious Diseases, [b]Department of Molecular Medicine II, [d]Cécile and Oskar Vogt Institute for Brain Research, and [f]Department of General Pediatrics, Neonatology, and Pediatric Cardiology, Heinrich Heine University Düsseldorf, 40225 Düsseldorf, Germany; [c]Institute of Immunology, Medical Faculty, University of Duisburg-Essen, 45147 Essen, Germany; and [e]Department of Physiology, University of Tübingen, 72076 Tübingen, Germany

Edited by Arthur J. L. Cooper, New York Medical College, Valhalla, NY, and accepted by the Editorial Board March 16, 2015 (received for review December 15, 2014)

Urea cycle defects and acute or chronic liver failure are linked to systemic hyperammonemia and often result in cerebral dysfunction and encephalopathy. Although an important role of the liver in ammonia metabolism is widely accepted, the role of ammonia metabolizing pathways in the liver for maintenance of whole-body ammonia homeostasis in vivo remains ill-defined. Here, we show by generation of liver-specific Gln synthetase (GS)-deficient mice that GS in the liver is critically involved in systemic ammonia homeostasis in vivo. Hepatic deletion of GS triggered systemic hyperammonemia, which was associated with cerebral oxidative stress as indicated by increased levels of oxidized RNA and enhanced protein Tyr nitration. Liver-specific GS-deficient mice showed increased locomotion, impaired fear memory, and a slightly reduced life span. In conclusion, the present observations highlight the importance of hepatic GS for maintenance of ammonia homeostasis and establish the liver-specific GS KO mouse as a model with which to study effects of chronic hyperammonemia.

hepatic encephalopathy | metabolic zonation | oxidative stress | RNA oxidation | glutamine

Hepatic ammonia and Gln metabolism are embedded into a structural/functional organization in the liver acinus, which allows efficient ammonia detoxification by the liver (1, 2). Hepatic urea synthesis in periportal hepatocytes is dependent on the activity of carbamoylphosphate synthetase, the rate-controlling enzyme of the urea cycle requiring ammonia as a substrate (3). The affinity of carbamoylphosphate synthetase for ammonia is low, and adequate flux through the urea cycle requires the establishment of high ammonia concentrations in periportal hepatocytes, which is achieved through ammonia amplification by periportal glutaminase activity (1–3). Excess ammonia not used by urea synthesis is taken up with high affinity by a small perivenous hepatocyte population (so-called "perivenous scavenger cells") (1), which detoxifies ammonia by amidation of Glu (4). This reaction is catalyzed by Gln synthetase (GS), which is specifically expressed in this small population of hepatocytes surrounding the terminal hepatic venule but not in other hepatocytes (4–6). This high-affinity ammonia removal by perivenous hepatocytes thus prevents spillover of hepatic ammonia into the systemic circulation. The acinar compartmentation of urea synthesis, Gln hydrolysis, and Gln synthesis therefore allows the generation of sizable ammonia concentrations in hepatic tissue needed for urea formation without the risk of toxic ammonia concentrations in systemic circulation (1).

Ammonia is toxic, particularly to the brain, where it can trigger hepatic encephalopathy (HE). HE is seen as the clinical manifestation of a low-grade cerebral edema with oxidative/nitrosative stress and subsequent derangements of signal transduction, neurotransmission, synaptic plasticity, and oscillatory networks in the brain (7–9). In particular, the oxidative/nitrosative stress response results in protein Tyr nitration (PTN) and RNA oxidation (9, 10). Astrocytes in close proximity to the blood–brain barrier exhibit strong PTN, possibly affecting its permeability (11). Data derived from HE animal models suggest a relationship between impaired functions of brain regions involved in cognition, learning, memory formation, and motor control, as well as elevated markers for oxidative stress in the hippocampus (12, 13), cerebral cortex (14), and cerebellum (15, 16). Consistently, increased markers for oxidative stress, such as PTN and RNA oxidation, have also been shown in postmortem human brain tissue of patients with liver cirrhosis and HE (17). In mice, ammonia can also inhibit potassium buffering by astrocytes, which results in increased extracellular potassium and may contribute to neuronal depolarization and dysfunction, and, consequently, altered behavior (18).

Liver damage can trigger defects in the ammonia metabolizing pathways, which consequently increase ammonia levels in circulating blood (19, 20). For example, LPS-induced liver injury results in PTN of hepatic GS, which inactivates the enzyme (21). The impact of the urea cycle for ammonia metabolism can be seen in children with urea cycle defects, who exhibit hyperammonemia and cognitive symptoms (22). In turn, hereditary GS deficiency in humans is a rare disorder leading to Gln deficiency and severe disease with a lethal outcome (23). Although destruction of perivenous hepatocytes by carbon tetrachloride intoxication impairs ammonia detoxification in perfused rat liver (24), the in vivo significance of the GS in perivenous hepatocytes has remained elusive. Because Gln can be synthesized in a wide variety of tissues

Significance

Ammonia metabolism in the liver is critical to prevent serious clinical conditions, such as hepatic encephalopathy. It was hypothesized that the Gln synthetase (GS) can metabolize ammonia with high affinity in the perivenous region of the liver. However, the in vivo relevance of this metabolic pathway remains unclear in view of other intra- and extrahepatic ammonia metabolizing pathways. Here, we show by creating a conditional GS KO mouse that specific deletion of the GS in the liver results in increased ammonia levels in the blood, induction of oxidative stress in brain tissue, and behavior abnormalities. In conclusion, GS in the liver is a key player in the maintenance of ammonia homeostasis.

Author contributions: D. Häussinger designed research; N.Q., P.A.L., B.G., V.I.P., M.P.O., K.S.L., H.J.B., E.L., C.B.L., and D. Herebian performed research; J.G.B., F.L., and D. Häussinger analyzed data; and N.Q., P.A.L., B.G., and D. Häussinger wrote the paper.

The authors declare no conflict of interest.

This article is a PNAS Direct Submission. A.J.L.C. is a guest editor invited by the Editorial Board.

[1]N.Q. and P.A.L. contributed equally to this work.

[2]To whom correspondence should be addressed. Email: haeussin@uni-duesseldorf.de.

This article contains supporting information online at www.pnas.org/lookup/suppl/doi:10.1073/pnas.1423968112/-/DCSupplemental.

PHYSIOLOGY

(4), specific deletion of hepatic GS would not be expected to result in Gln deficiency. However, lack of hepatic GS may disrupt perivenous ammonia metabolism, thus leading to increased ammonia concentrations in systemic blood.

To test this hypothesis, gene-targeted mice lacking functional hepatic GS were generated and analyzed. As a result of liver-specific GS deletion, mice developed systemic hyperammonemia, which was accompanied by cerebral RNA oxidation, PTN, motoric and behavioral abnormalities, and a reduced life span.

Results

Effect of Liver-Specific GS Deletion on Liver Tissue Integrity, Zonation, and Systemic Ammonia Levels. Liver injury can result in a reduction of hepatic GS activity (21, 24). Because other potent ammonia detoxicating mechanisms exist in the body, the role of the GS in perivenous liver cells remains controversial. To investigate the role of GS, we created conditional GS KO mice (Fig. 1*A*), which were crossed with a mouse strain where Cre is expressed under the albumin promotor (25). As expected, GS was strongly expressed in liver tissue in locus of X-over P1 (loxP) sites flanked by glutamate-

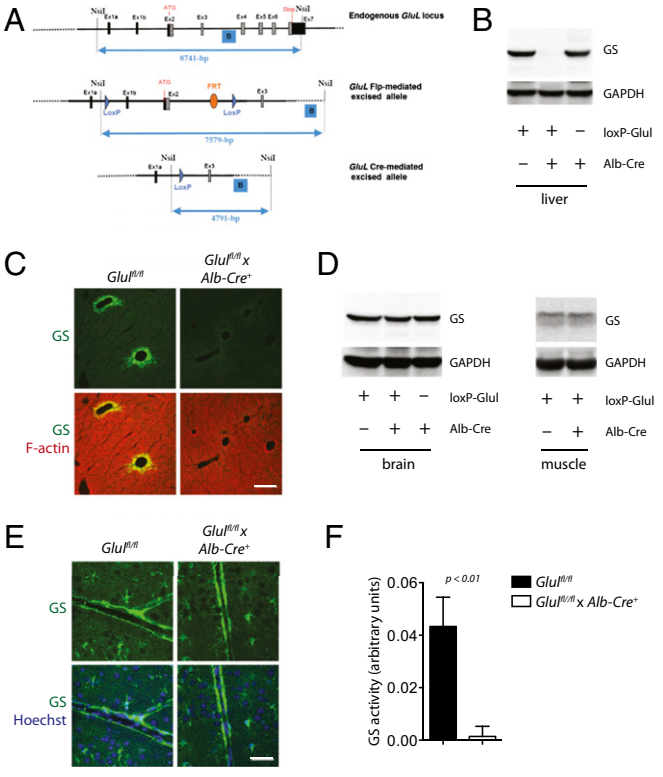

Fig. 1. Organ-specific deletion of GS in the *Glul*$^{fl/fl}$ × *Alb-Cre*$^{+}$ mice. (*A*) Gene-targeted mice lacking functional hepatic GS were generated as described in *Materials and Methods*. (*B*) GS and GAPDH expression in liver tissue from *Glul*$^{fl/fl}$ × *Alb-Cre*$^{+}$, *Alb-Cre*$^{+}$, and *Glul*$^{fl/fl}$ mice is shown using Western blot analysis. One representative of $n = 3$ is shown. (*C*) Snap-frozen sections from liver tissue harvested from *Alb-Cre*$^{+}$, *Glul*$^{fl/fl}$, and *Glul*$^{fl/fl}$ × *Alb-Cre*$^{+}$ mice were stained with anti-GS (green) and F-actin (red) antibodies. One representative of $n = 3$ is shown. (Scale bar: 200 μm.) (*D*, *Left*) Western blot analysis for GS and GAPDH on protein samples obtained from brain tissue from *Glul*$^{fl/fl}$ × *Alb-Cre*$^{+}$, *Alb-Cre*$^{+}$, and *Glul*$^{fl/fl}$ mice was performed. (*D*, *Right*) GS expression and GAPDH expression were assessed in muscle tissue of *Glul*$^{fl/fl}$ × *Alb-Cre*$^{+}$ and *Glul*$^{fl/fl}$ mice by Western blot analysis. One representative of $n = 3$ is shown. (*E*) Immunostaining of snap-frozen sections from brain tissue harvested from *Alb-Cre*$^{+}$, *Glul*$^{fl/fl}$, and *Glul*$^{fl/fl}$ × *Alb-Cre*$^{+}$ mice with an anti-GS antibody (green) and Hoechst 34580 (blue) was performed. One representative of $n = 3$ is shown. (Scale bar: 50 μm.) (*F*) GS activity was assessed in liver tissue harvested from *Glul*$^{fl/fl}$ and *Glul*$^{fl/fl}$ × *Alb-Cre*$^{+}$ mice ($n = 3$–7, respectively).

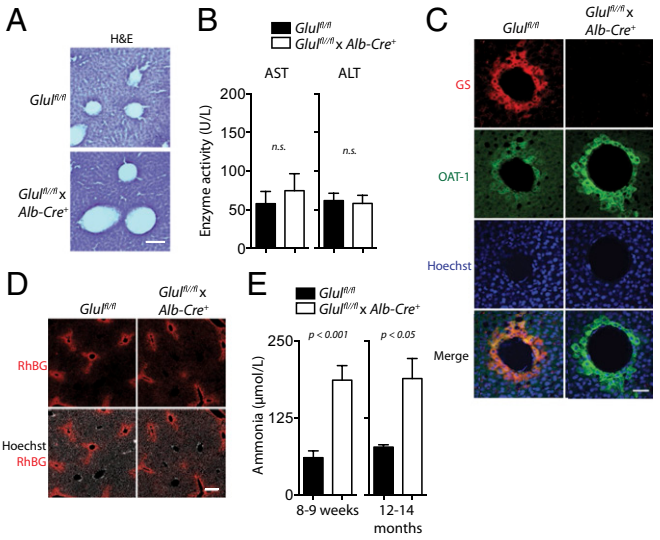

Fig. 2. Intact liver architecture/zonation and elevated systemic ammonia levels by liver-specific deletion of GS. (*A*) Representative H&E-stained sections of snap-frozen liver tissue obtained from *Glul*$^{fl/fl}$ × *Alb-Cre*$^{+}$ and *Glul*$^{fl/fl}$ mice of $n = 3$ is shown. (Scale bar: 100 μm.) (*B*) Asp aminotransferase (AST) and Ala aminotransferase (ALT) activity was determined in the serum of *Glul*$^{fl/fl}$ ($n = 10$) and *Glul*$^{fl/fl}$ × *Alb-Cre*$^{+}$ mice ($n = 12$). n.s., not statistically significantly different. (*C*) Immunofluorescence analyses of snap-frozen liver tissue from *Glul*$^{fl/fl}$ × *Alb-Cre*$^{+}$ (*Lower*) and *Glul*$^{fl/fl}$ (*Upper*) mice were performed for GS (red), ornithine aminotransferase (OAT; green), and Hoechst 34580 (blue). One representative set of images of $n = 3$ is shown. (Scale bar: 20 μm.) (*D*) Immunofluorescence analyses of snap-frozen liver tissue from *Glul*$^{fl/fl}$ × *Alb-Cre*$^{+}$ (*Right*) and *Glul*$^{fl/fl}$ (*Left*) mice were performed for ammonia transporter Rh family B glycoprotein (RhBG; red) and Hoechst 34580 (gray). One representative set of images of $n = 3$ (*Glul*$^{fl/fl}$) and $n = 4$ (*Glul*$^{fl/fl}$ × *Alb-Cre*$^{+}$) is shown. (Scale bar: 200 μm.) (*E*) Ammonia levels were assessed in blood samples collected by cardiac puncture from 8- to 9-wk-old *Glul*$^{fl/fl}$ × *Alb-Cre*$^{+}$ mice and *Glul*$^{fl/fl}$ mice (*Left*, $n = 7$–8, respectively) and from 12- to 14-month-old animals (*Right*, $n = 3$).

ammonia ligase gene (*Glul*$^{fl/fl}$) mice in the absence of Cre recombinase but was undetectable in *Glul*$^{fl/fl}$ × albumin promoter-controlled Cre recombinase gene (*Alb-Cre*$^{+}$) mice (Fig. 1 *B* and *C*). Deletion of GS in the liver did not affect GS expression in the brain or in muscle tissue (Fig. 1 *D* and *E*). GS activity was high in liver tissue from *Glul*$^{fl/fl}$ mice, whereas only residual GS activity was detected in liver tissue from *Glul*$^{fl/fl}$ × *Alb-Cre*$^{+}$ mice (Fig. 1*F*), which is probably attributable to tissue resident macrophages (26). Next, we investigated whether hepatic deletion of GS affected liver architecture or damage. Histologically, no difference between WT and *Glul*$^{fl/fl}$ × *Alb-Cre*$^{+}$ mice in snap-frozen liver sections was observed (Fig. 2*A*). Furthermore, activities of Asp and Ala aminotransferases in serum were not different between WT and KO mice, indicating that the absence of hepatic GS did not result in liver damage (Fig. 2*B*). Although GS was selectively deleted in perivenous hepatocytes (Fig. 2*C*), ornithine aminotransferase (OAT), as well as Rhesus family B glycoprotein, which show similar acinar localization as GS, were still detectable in these specialized cells (27, 28) (Fig. 2 *C* and *D*). These data indicated that the zonal organization of the liver was not affected by the liver-specific GS KO. However, when we checked blood ammonia levels, strongly elevated ammonia concentrations were observed in blood plasma from KO mice compared with WT mice (Fig. 2*E*). This increase in plasma ammonia concentration was probably not due to a urea cycle defect, because expression of genes encoding for enzymes of the urea cycle in the liver was similar in WT and *Glul*$^{fl/fl}$ × *Alb-Cre*$^{+}$ mice (Fig. S1*A*). Moreover, serum urea nitrogen concentrations did not differ between WT and *Glul*$^{fl/fl}$ × *Alb-Cre*$^{+}$ mice (Fig. S1*B*). Furthermore, serum Gln, Glu, and Ala

concentrations were not significantly different between *Glul*$^{fl/fl}$ and *Glul*$^{fl/fl}$ × *Alb-Cre*$^{+}$ mice (Fig. S1*C*). Taken together, these data indicate that liver-specific deletion of GS does not affect liver architecture but allows ammonia spillover into the systemic circulation, thereby leading to hyperammonemia.

Liver-Specific GS KO Triggers PTN and RNA Oxidation in Mouse Brain. Ammonia intoxication and HE were shown to trigger PTN nitration and RNA oxidation in the rat and human brain, respectively (10, 17, 21, 29). Therefore, we analyzed whether these effects could also be observed in brain tissue from liver-specific GS KO mice. Whereas PTN was enhanced in the cerebellum, hippocampus, and somatosensory cortex of *Glul*$^{fl/fl}$ × *Alb-Cre*$^{+}$ mice (Fig. 3 *A*–*C*), it was similar to PTN in WT mice in the piriform cortex (Fig. 3*D*).

Thus, nitration of proteins due to chronic ammonia intoxication affects specific regions of the brain (Fig. 3*E*). Next, we investigated whether RNA oxidation was present in brain tissue using immunofluorescence. As evidenced by anti–8-hydroxy-2-(de)oxyguanosine [8-OH(d)G] immunoreactivity, RNA oxidation was consistently found in the cerebellum, hippocampus, and somatosensory cortex (Fig. 4 *A*–*C*) but not in the piriform cortex (Fig. 4*D*). When brain slices were treated with RNase, no anti–8-OH(d)G immunoreactivity was detectable on the brain slices, indicating that the oxidation was specific for RNA (Fig. S2). These results were also confirmed with Northwestern blotting (Fig. 4*E* and Fig. S3 *A*–*D*). Interestingly, in the cerebellum of mice lacking hepatic GS, we identified exceptionally high levels of oxidized RNA in Purkinje cells (Fig. S4), which critically control motor functions (30). Taken together, specific deletion of GS in the liver results in increased ammonia levels and, consequently, biochemical changes in brain tissue of *Glul*$^{fl/fl}$ × *Alb-Cre*$^{+}$ mice.

***Glul*$^{fl/fl}$ × *Alb-Cre*$^{+}$ Mice Show No Microglia Activation in Mouse Cerebral Cortex.** Microglia activation was shown in the brain of animal models for acute and chronic liver failure (16, 31) and in human postmortem brain samples from patients with liver cirrhosis and HE (32). However, microglia activation markers, such as ionized calcium-binding adaptor protein 1 (Iba1) expression, and microglia morphology, were unchanged in the cerebral cortex of *Glul*$^{fl/fl}$ × *Alb-Cre*$^{+}$ mice compared with WT mice (Fig. 5*A*). In line with this finding, cerebrocortical Iba1 and CD14 mRNA (Fig. 5*B*) and protein (Fig. S5*A*) levels were unchanged in *Glul*$^{fl/fl}$ × *Alb-Cre*$^{+}$ mice compared with *Glul*$^{fl/fl}$ mice. In the brain, proinflammatory cytokines are largely synthesized by activated microglia (33). Also, mRNA (Fig. 5*C*) and protein (Fig. S5*B*) levels of the proinflammatory cytokines IL-1β, IL-6, and TNF-α remained unchanged in the cerebral cortex of *Glul*$^{fl/fl}$ × *Alb-Cre*$^{+}$ mice compared with *Glul*$^{fl/fl}$ mice. These data suggest that systemic hyperammonemia in *Glul*$^{fl/fl}$ × *Alb-Cre*$^{+}$ mice is not associated with microglia activation and increased synthesis of proinflammatory cytokines in cerebral cortex.

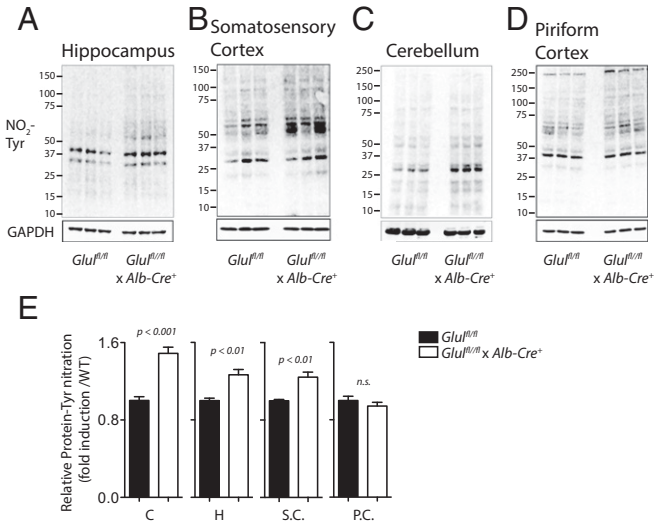

Fig. 3. Hepatic GS KO triggers PTN in mouse brain. Protein samples harvested from brain slices of the cerebellum, hippocampus, somatosensory cortex, and piriform cortex of *Glul*$^{fl/fl}$ and *Glul*$^{fl/fl}$ × *Alb-Cre*$^{+}$ mice were tested for PTN using Western blot analysis. (*A*–*D*, *Upper*) Representative blots showing anti–3′-nitrotyrosine immunoreactivity. (*A*–*D*, *Lower*) GAPDH served as a loading control. (*E*) Mean ± SEM of the densitometry of the cerebellum (C), hippocampus (H), somatosensory cortex (S.C.), and cortex piriform (C.P.) is presented ($n = 6$ for *Glul*$^{fl/fl}$ and $n = 9$ for *Glul*$^{fl/fl}$ × *Alb-Cre*$^{+}$ mice for the cerebellum and hippocampus, $n = 6$ for *Glul*$^{fl/fl}$ and $n = 8$ for *Glul*$^{fl/fl}$ × *Alb-Cre*$^{+}$ mice for the somatosensory cortex, and $n = 3$ for *Glul*$^{fl/fl}$ and $n = 6$ for *Glul*$^{fl/fl}$ × *Alb-Cre*$^{+}$ mice for the cortex piriform).

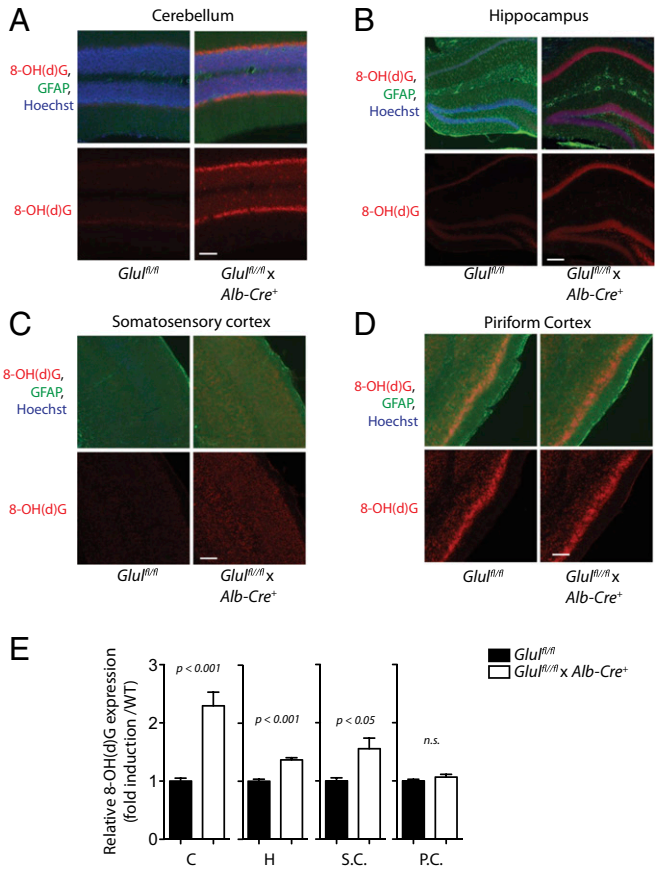

Fig. 4. Liver-specific deletion of GS induces RNA oxidation in mouse brain. (*A*–*D*) Survey of 8-OH(d)G immunoreactivity in brain tissue from *Glul*$^{fl/fl}$ (*Left*) and *Glul*$^{fl/fl}$ × *Alb-Cre*$^{+}$ (*Right*) mice is presented in the absence (*Lower*) or presence (*Upper*) of costaining with GFAP (green) and Hoechst 34580 (blue). One representative of the cerebellum (*A*), hippocampus (*B*), somatosensory cortex (*C*), and piriform cortex (*D*) of $n = 5$ is demonstrated. (Scale bars: *A*, 100 μm; *B*–*D*, 200 μm.) (*E*) Samples harvested from brain sections (from left to right: cerebellum, hippocampus, somatosensory cortex, and piriform cortex) of *Glul*$^{fl/fl}$ and *Glul*$^{fl/fl}$ × *Alb-Cre*$^{+}$ mice were tested for RNA oxidation expression using Northwestern blotting [$n = 6$ for *Glul*$^{fl/fl}$ mice, $n = 9$ (cerebellum, hippocampus, and piriform cortex) and $n = 10$ (somatosensory cortex) for *Glul*$^{fl/fl}$ × *Alb-Cre*$^{+}$ mice].

***Glul*$^{fl/fl}$ × *Alb-Cre*$^{+}$ Mice Exhibit Behavioral Abnormalities.** Changes in ammonia levels in patients can trigger signs of HE. We therefore tested whether liver-specific deletion of GS resulted in behavioral abnormalities. Interestingly, when we monitored animal activity using light barrier-equipped cages, increased activity of

PHYSIOLOGY

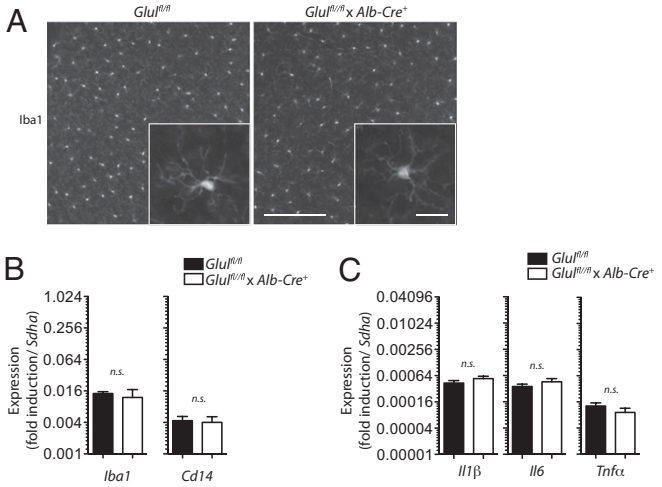

Fig. 5. Microglia activation marker and proinflammatory cytokine mRNA expression in the cerebral cortex of WT and *Glul*$^{fl/fl}$ × *Alb-Cre*$^{+}$ mice. (*A*) Detection of Iba1 in mouse cerebral cortex by wide-field fluorescence microscopy. One representative immunofluorescence analysis of three is shown. (Scale bars: 200 μm; *Inset*, 20 μm.) mRNA expression levels in mouse cerebral cortex by RT-PCR of Iba1 and CD14 (*B*, $n = 3$) or IL-1β, I-L6, or TNF-α (*C*, $n = 8$ for *Glul*$^{fl/fl}$ mice and $n = 6$ of for *Glul*$^{fl/fl}$ × *Alb-Cre*$^{+}$ mice) are shown. mRNA expression levels of Iba1, CD14, IL-1β, IL-6, or TNF-α were normalized to succinate dehydrogenase complex subunit A (SDHA) mRNA levels.

Glul$^{fl/fl}$ × *Alb-Cre*$^{+}$ mice compared with WT mice was observed (Fig. 6*A*). Consistently, the overall distance traveled by *Glul*$^{fl/fl}$ × *Alb-Cre*$^{+}$ mice was increased compared with *Glul*$^{fl/fl}$ mice (Fig. 6*B*). Furthermore, using the O-Maze test, *Glul*$^{fl/fl}$ × *Alb-Cre*$^{+}$ mice spent more time in the open arms compared with control animals (Fig. 6*C*). In turn, *Glul*$^{fl/fl}$ × *Alb-Cre*$^{+}$ mice spent less time in the protected arms than *Glul*$^{fl/fl}$ mice (Fig. 6*D*). Taken together, these data indicate that chronic hyperammonemia results in behavioral abnormalities. Furthermore, when we monitored the WT and *Glul*$^{fl/fl}$ × *Alb-Cre*$^{+}$ mice over time, we observed slightly reduced survival of GS-deficient mice compared with WT controls (Fig. S6), indicating that chronic ammonia exposure may reduce the life span in vivo. Taken together, these data indicate that deletion of GS in the liver results in hyperammonemia, phenotypic changes in brain tissue, and behavioral abnormalities.

Discussion

According to the present observations, lack of hepatic GS is followed by a marked increase of plasma ammonia levels. Hepatic GS is selectively expressed in a small population of perivenous hepatocytes (4–6, 34, 35). This expression pattern depends on Wnt-mediated activation of the transcriptional coactivator β-catenin (36, 37), which is also involved in hepatocyte proliferation (38–40). Consequently, liver-specific β-catenin–deficient mice exhibit defective GS activity in the liver (36). In our study, the severe hyperammonemia of the *Glul*$^{fl/fl}$ × *Alb-Cre*$^{+}$ mice highlights the importance of this enzyme in a small population of perivenous hepatocytes (so-called "perivenous scavenger cells") as a high-affinity ammonia scavenger, which prevents ammonia spillover from the periportal urea-synthesizing compartment into the systemic circulation. The present observations show the in vivo relevance of a hypothesis postulated almost three decades ago (1, 2, 24). As illustrated in Figs. 1*C* and 2*C*, the enzyme is specifically expressed in a small subpopulation of perivenous hepatocytes and is completely absent in the remainder of liver parenchyma. Thus, expression of the enzyme in this small population of hepatocytes, which amounts to only 6–7% of all liver parenchymal cells (5), is pivotal for the maintenance of nontoxic ammonia levels in the organism. The hyperammonemia in hepatic failure is thus not simply the result of impaired urea formation but may, in large part, result from an impaired ability of the perivenous cells to incorporate ammonia into Gln. Apart from perivenous hepatocytes, several other cell types, including skeletal muscle, can take up ammonia, and thus contribute to ammonia detoxification (41). However, extrahepatic GS, which is intact in *Glul*$^{fl/fl}$ × *Alb-Cre*$^{+}$ mice, is apparently not sufficient to prevent hyperammonemia in arterial blood and to compensate for the lack of GS in the liver.

The safeguard of perivenous ammonia detoxification allows the periportal hepatocytes to generate ammonia by Gln hydrolysis as a substrate for periportal urea synthesis, which is a low-affinity system for ammonia detoxification (1). The ammonia generated by hepatic glutaminase, which is expressed in periportal hepatocytes, adds to the ammonia generated in the gastrointestinal tract. Such high ammonia concentrations are apparently tolerated by hepatocytes but are toxic to the brain (42). Arterial ammonia readily crosses the blood–brain barrier, thus entering cerebral tissue (43). In the brain, ammonia leads to Gln formation, astrocyte swelling, and generation of reactive oxygen and nitrogen species. Astrocyte swelling and oxidative/nitrosative stress affect signal transduction, neurotransmission, synaptic plasticity, and oscillatory networks in the brain (42). The present observations revealed enhanced PTN and RNA oxidation in brain regions of *Glul*$^{fl/fl}$ × *Alb-Cre*$^{+}$ mice, whose function is compromised in HE. Functions affected in HE include memory formation in the hippocampus (44); processing of sensory stimuli, such as perception, in the somatosensory cortex (45); and motor functions in the cerebellum (46). Interestingly, in the cerebellum of mice lacking hepatic GS, we identified exceptionally high levels of oxidized RNA in Purkinje cells, which critically control motor functions (30). In line with deranged cerebral motor control, the present study identified increased locomotion in mice lacking hepatic GS with liver damage and/or cholestasis due to bile duct ligation (47, 48), portocaval shunting (49), or portal vein ligation (14). This difference may suggest a role of impaired liver metabolism other than ammonia detoxification for decreased locomotion in these HE animal models. One may also speculate that

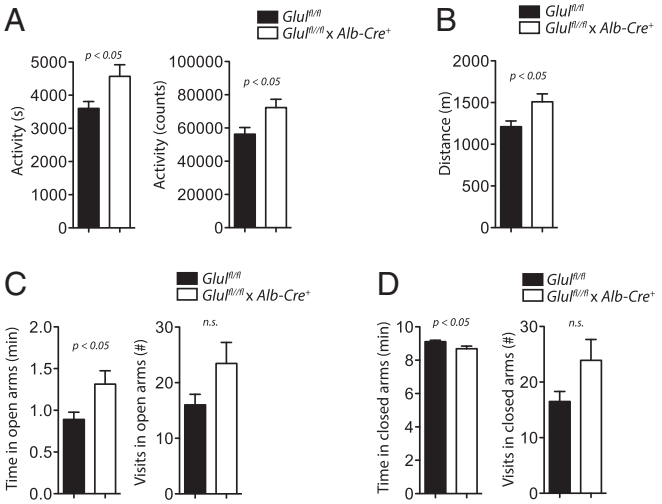

Fig. 6. *Glul*$^{fl/fl}$ × *Alb-Cre*$^{+}$ mice show behavioral abnormalities compared with WT mice. (*A* and *B*) *Glul*$^{fl/fl}$ and *Glul*$^{fl/fl}$ × *Alb-Cre*$^{+}$ mice were transferred into a light barrier-equipped cage and allowed to adapt to the new environment for 24 h prior to starting the measurement. Total activity time (*Left*, $n = 22$ for *Glul*$^{fl/fl}$ mice and $n = 23$ for *Glul*$^{fl/fl}$ × *Alb-Cre*$^{+}$ mice) and counts (*Right*, $n = 23$ for *Glul*$^{fl/fl}$ mice and $n = 24$ for *Glul*$^{fl/fl}$ × *Alb-Cre*$^{+}$ mice) (*A*) and distance traveled ($n = 21$ for *Glul*$^{fl/fl}$ mice and $n = 22$ for *Glul*$^{fl/fl}$ × *Alb-Cre*$^{+}$ mice) (*B*) were determined after 24 h. Animals were monitored using the O-Maze test. Time (*Left*) and visits (*Right*) in the open arms (*C*) and time (*Left*) and visits (*Right*) in the closed arms (*D*) are presented ($n = 10$ for *Glul*$^{fl/fl}$ mice and $n = 11$ for *Glul*$^{fl/fl}$ × *Alb-Cre*$^{+}$ mice).

chronic hyperammonemia from birth in $Glul^{fl/fl} \times Alb\text{-}Cre^{+}$ mice may trigger so far unknown adaptations that are not present in other experimental settings or in patients with liver failure. However, that chronic hyperammonemia in $Glul^{fl/fl} \times Alb\text{-}Cre^{+}$ mice does not promote anxious behavior is consistent with findings obtained from bile duct-ligated rats (47) or rats after portocaval anastomosis (50). Interestingly, oxidative stress markers were not elevated in the piriform cortex of liver-specific GS KO mice. Presently, the underlying reason, as well as the functional significance of this finding, remains enigmatic and needs to be explored in further studies.

Our findings also demonstrate that chronic hyperammonemia in this mouse model is not sufficient to activate microglia in the cerebral cortex, which contrasts with findings on mouse brain after acute liver failure due to liver ischemia or intoxication (51) or findings on human brain tissue from cirrhotic patients with HE (32, 52). These discrepancies may be explained by species differences, allowance for compensatory mechanisms in chronic hyperammonemia, and/or the complexity or severity of the pathophysiological setting in humans with liver cirrhosis. Therefore, other factors, such as systemic inflammation in acute liver failure (51) and HE (53), might contribute to cerebral microglia activation in HE (32, 52). Indeed, a recent transcriptome analysis on postmortem human brain samples indicated that systemic inflammation may trigger altered cerebral expression of genes involved in inflammation in patients with liver cirrhosis and HE (52). Furthermore, our results demonstrate that cerebral synthesis of proinflammatory cytokines as observed in some animal models for HE is not solely explained by hyperammonemia (16, 31), in line with previous data (13, 14). Consistent with the present findings, data derived from postmortem human brain samples consistently show no up-regulation of proinflammatory cytokine mRNA or protein in the brain tissue of patients with liver cirrhosis and HE (32, 52, 54).

As shown in this paper, expression of functional GS in the perivenous hepatic scavenger cell population is critical for ammonia homeostasis in vivo. Liver cirrhosis in animal models and man and hepatocellular carcinoma are associated with strongly reduced GS activity, followed by hyperammonemia (2, 55–57). In cirrhosis with collaterals, down-regulation of GS in scavenger cells may be related to portocaval shunting (3, 58, 59). Here, it should be noted that glutaminase activity in the cirrhotic liver increases four- to fivefold to compensate for a marked reduction of the capacity for urea synthesis, thereby maintaining a life-compatible urea cycle flux (55). Clinical conditions such as sepsis (21) or portocaval anastomosis (58) are associated with reduced GS activity as a consequence of a scavenger cell defect, although flux through periportal urea synthesis is not affected.

The crucial role of hepatic GS for the maintenance of ammonia homeostasis as shown in the present study is also supported by a recent study using muscle-specific GS KO mice, where arterial ammonia levels were only marginally elevated compared with $Glul^{fl/fl}$ mice (60). Here, it was concluded that skeletal muscle may only contribute about 3% of daily whole-body ammonia detoxification. Moreover, our study shows no compensatory up-regulation of GS in skeletal muscle in $Glul^{fl/fl} \times Alb\text{-}Cre^{+}$ mice. Notably, the chronic hyperammonemia from birth in the absence of liver damage in $Glul^{fl/fl} \times Alb\text{-}Cre^{+}$ mice may resemble hyperammonemia in children with inborn urea cycle disorders, who also exhibit cognitive and motor deficits (22). These disorders emphasize the importance of the urea cycle for ammonia clearance. Accordingly, both the high-affinity and low-affinity systems represent two independent primary systems in the liver for ammonia removal.

In conclusion, the present study shows that lack of GS activity in a small subpopulation of perivenous hepatocytes leads to hyperammonemia and cerebral ammonia intoxication.

Materials and Methods

Animals. Gene-targeted mice lacking functional hepatic GS were generated by inserting a loxP site, together with a flip-recombinase target flanked neomycin resistance cassette, downstream of the 3′ end of exon 3 and a single loxP site between exon 1a and exon 1b (GenOway; Fig. 1*A*). Resulting mice were crossed with deleter mice expressing the flippase recombinase to remove the resistance cassette. $Glul^{fl/fl}$ mice were backcrossed to C57BL/6J background more than 10 times. Next, mice were crossed to a mouse expressing the Cre recombinase under the albumin promotor (25), resulting in liver-specific deletion of GS. Animals appeared viable and fertile, and showed no signs of distress. Animals were kept under specific pathogen-free conditions. Age- and sex-matched animals weighing over 20 g were used for experiments. Most experiments were carried out with littermate controls of mice aged between 8 and 12 wk. For determination of locomotor activity, animals between 3 and 75 wk of age were transferred into a light barrier-equipped cage monitored by a computer system (ActiMot/MoTil; TSE-Systems). Animals were allowed to adapt to the new environment for 24 h prior to starting the measurement for another 24 h. All animal experiments were reviewed and approved by the appropriate authorities, and were performed in accordance with the German animal protection law (Landesamt für Natur, Umwelt und Verbraucherschutz Recklinghausen, Regierungspräsidium Tübingen, Tierveruchsanlage Düsseldorf). Genotyping and the O-Maze test of mice were performed as described in *SI Materials and Methods*.

Tissue Sampling. Detailed information on tissue sampling is provided in *SI Materials and Methods*. The cerebral cortex was further dissected due to visible morphological characteristics (61).

Video-Tracking. For data acquisition, animals were video-tracked by a 302050-SW-KIT-2-CAM camera (TSE-Systems) at a resolution of 0.62–0.72 pixel and analyzed using the tracking software VideoMot2 (TSE-Systems).

Western Blot Analysis. Western blot analysis was carried out as described in *SI Materials and Methods* and previously (11).

Northwestern Blot Analysis. Northwestern blot analysis was carried out as described in *SI Materials and Methods* and previously (10).

Immunofluorescence Analysis. Immunofluorescence analysis was carried out as described in *SI Materials and Methods* and previously (10).

GS Activity Assay. GS activity was measured according to the γ-glutamyl transferase reaction as described recently (21) and in *SI Materials and Methods*.

Real-Time PCR. Quantitative real-time PCR is described in detail in *SI Materials and Methods*, including PCR primer sequences.

Serum Liver Enzyme Activity. Activity of Ala aminotransferase and Asp aminotransferase was measured in serum using a serum multiple biochemical analyzer (Ektachem DTSCII; Johnson & Johnson).

Quantification of Urea Nitrogen in Serum and Urine. Urea nitrogen was quantified using a Spotchem analyzer (Axonlab). Serum samples were prediluted 1:5 and urine samples were prediluted 1:50 in PBS (Panbiotech).

Blood Ammonia Determination. Blood ammonia was measured within 3 min after blood sampling from the right heart ventricle using an Ammonia Checker II (Daiichi Kagaku Co. Ltd., distributed by Nobis Labordiagnostica GmbH).

Statistical Analysis. Data are provided as means ± SEM, and n represents the number of animals tested. All data were tested for significance using a paired or unpaired Student's t test or one-way ANOVA. Only results with $P < 0.05$ were considered statistically significant.

ACKNOWLEDGMENTS. This study was supported by the Deutsche Forschungsgemeinschaft through Collaborative Research Centers Grant Sonderforschungsbereich (SFB) 575 "Experimental Hepatology" (Düsseldorf) and Grant SFB 974 "Communication and Systems Relevance of Liver Injury and Regeneration" (Düsseldorf), the Alexander von Humboldt Foundation (Grant SKA2010), and the in vivo investigations in metabolic pathomechanisms and diseases in Düsseldorf Graduate School of the Heinrich Heine University of Düsseldorf.

1. Häussinger D (1983) Hepatocyte heterogeneity in glutamine and ammonia metabolism and the role of an intercellular glutamine cycle during ureogenesis in perfused rat liver. *Eur J Biochem* 133(2):269–275.
2. Häussinger D (1990) Nitrogen metabolism in liver: Structural and functional organization and physiological relevance. *Biochem J* 267(2):281–290.
3. Häussinger D, Lamers WH, Moorman AF (1992) Hepatocyte heterogeneity in the metabolism of amino acids and ammonia. *Enzyme* 46(1-3):72–93.
4. Häussinger D, Schliess F (2007) Glutamine metabolism and signaling in the liver. *Front Biosci* 12:371–391.
5. Gebhardt R, Mecke D (1983) Heterogeneous distribution of glutamine synthetase among rat liver parenchymal cells in situ and in primary culture. *EMBO J* 2(4):567–570.
6. Gaasbeek Janzen JW, et al. (1984) Immunohistochemical localization of carbamoylphosphate synthetase (ammonia) in adult rat liver; evidence for a heterogeneous distribution. *J Histochem Cytochem* 32(6):557–564.
7. Häussinger D, Sies H (2013) Hepatic encephalopathy: Clinical aspects and pathogenetic concept. *Arch Biochem Biophys* 536(2):97–100.
8. Norenberg MD, et al. (1991) Ammonia-induced astrocyte swelling in primary culture. *Neurochem Res* 16(7):833–836.
9. Häussinger D, Schliess F (2008) Pathogenetic mechanisms of hepatic encephalopathy. *Gut* 57(8):1156–1165.
10. Görg B, et al. (2008) Ammonia induces RNA oxidation in cultured astrocytes and brain in vivo. *Hepatology* 48(2):567–579.
11. Schliess F, et al. (2002) Ammonia induces MK-801-sensitive nitration and phosphorylation of protein tyrosine residues in rat astrocytes. *FASEB J* 16(7):739–741.
12. Roselló DM, et al. (2008) Oxidative stress and hippocampus in a low-grade hepatic encephalopathy model: Protective effects of curcumin. *Hepatol Res* 38(11):1148–1153.
13. Begega A, et al. (2010) Portal hypertension in 18-month-old rats: Memory deficits and brain metabolic activity. *Physiol Behav* 100(2):135–142.
14. Brück J, et al. (2011) Locomotor impairment and cerebrocortical oxidative stress in portal vein ligated rats in vivo. *J Hepatol* 54(2):251–257.
15. Dhanda S, Kaur S, Sandhir R (2013) Preventive effect of N-acetyl-L-cysteine on oxidative stress and cognitive impairment in hepatic encephalopathy following bile duct ligation. *Free Radic Biol Med* 56:204–215.
16. Rodrigo R, et al. (2010) Hyperammonemia induces neuroinflammation that contributes to cognitive impairment in rats with hepatic encephalopathy. *Gastroenterology* 139(2):675–684.
17. Görg B, et al. (2010) Oxidative stress markers in the brain of patients with cirrhosis and hepatic encephalopathy. *Hepatology* 52(1):256–265.
18. Rangroo Thrane V, et al. (2013) Ammonia triggers neuronal disinhibition and seizures by impairing astrocyte potassium buffering. *Nat Med* 19(12):1643–1648.
19. Seifert G, Schilling K, Steinhäuser C (2006) Astrocyte dysfunction in neurological disorders: A molecular perspective. *Nat Rev Neurosci* 7(3):194–206.
20. Häussinger D, Sies H, Gerok W (1985) Functional hepatocyte heterogeneity in ammonia metabolism. The intercellular glutamine cycle. *J Hepatol* 1(1):3–14.
21. Görg B, Wettstein M, Metzger S, Schliess F, Häussinger D (2005) Lipopolysaccharide-induced tyrosine nitration and inactivation of hepatic glutamine synthetase in the rat. *Hepatology* 41(5):1065–1073.
22. Gropman AL, Batshaw ML (2004) Cognitive outcome in urea cycle disorders. *Mol Genet Metab* 81(Suppl 1):S58–S62.
23. Häberle J, et al. (2005) Congenital glutamine deficiency with glutamine synthetase mutations. *N Engl J Med* 353(18):1926–1933.
24. Häussinger D, Gerok W (1984) Hepatocyte heterogeneity in ammonia metabolism: Impairment of glutamine synthesis in CCl4 induced liver cell necrosis with no effect on urea synthesis. *Chem Biol Interact* 48(2):191–194.
25. Postic C, et al. (1999) Dual roles for glucokinase in glucose homeostasis as determined by liver and pancreatic beta cell-specific gene knock-outs using Cre recombinase. *J Biol Chem* 274(1):305–315.
26. Bode JG, Peters-Regehr T, Kubitz R, Häussinger D (2000) Expression of glutamine synthetase in macrophages. *J Histochem Cytochem* 48(3):415–422.
27. Kuo FC, Hwu WL, Valle D, Darnell JE, Jr (1991) Colocalization in pericentral hepatocytes in adult mice and similarity in developmental expression pattern of ornithine aminotransferase and glutamine synthetase mRNA. *Proc Natl Acad Sci USA* 88(21):9468–9472.
28. Weiner ID, Miller RT, Verlander JW (2003) Localization of the ammonium transporters, Rh B glycoprotein and Rh C glycoprotein, in the mouse liver. *Gastroenterology* 124(5):1432–1440.
29. Görg B, et al. (2007) Reversible inhibition of mammalian glutamine synthetase by tyrosine nitration. *FEBS Lett* 581(1):84–90.
30. Barski J, et al. (2003) Calbindin in cerebellar Purkinje cells is a critical determinant of the precision of motor coordination. *J Neurosci* 23(8):3469–3477.
31. Jiang W, Desjardins P, Butterworth RF (2009) Direct evidence for central proinflammatory mechanisms in rats with experimental acute liver failure: Protective effect of hypothermia. *J Cereb Blood Flow Metab* 29(5):944–952.
32. Zemtsova I, et al. (2011) Microglia activation in hepatic encephalopathy in rats and humans. *Hepatology* 54(1):204–215.
33. Glass CK, Saijo K, Winner B, Marchetto MC, Gage FH (2010) Mechanisms underlying inflammation in neurodegeneration. *Cell* 140(6):918–934.
34. Burke ZD, et al. (2009) Liver zonation occurs through a beta-catenin-dependent, c-Myc-independent mechanism. *Gastroenterology* 136(7):2316–2324. e1–e3.
35. Clinkenbeard EL, Butler JE, Spear BT (2012) Pericentral activity of alpha-fetoprotein enhancer 3 and glutamine synthetase upstream enhancer in the adult liver are regulated by β-catenin in mice. *Hepatology* 56(5):1892–1901.
36. Sekine S, Lan BY-A, Bedolli M, Feng S, Hebrok M (2006) Liver-specific loss of beta-catenin blocks glutamine synthesis pathway activity and cytochrome p450 expression in mice. *Hepatology* 43(4):817–825.
37. Yang J, et al. (2014) β-catenin signaling in murine liver zonation and regeneration: A Wnt-Wnt situation! *Hepatology* 60(3):964–976.
38. Sekine S, Gutiérrez PJA, Lan BY-A, Feng S, Hebrok M (2007) Liver-specific loss of beta-catenin results in delayed hepatocyte proliferation after partial hepatectomy. *Hepatology* 45(2):361–368.
39. Tan X, Behari J, Cieply B, Michalopoulos GK, Monga SPS (2006) Conditional deletion of beta-catenin reveals its role in liver growth and regeneration. *Gastroenterology* 131(5):1561–1572.
40. Nejak-Bowen KN, et al. (2010) Accelerated liver regeneration and hepatocarcinogenesis in mice overexpressing serine-45 mutant beta-catenin. *Hepatology* 51(5):1603–1613.
41. Dam G, Ott P, Aagaard NK, Vilstrup H (2013) Branched-chain amino acids and muscle ammonia detoxification in cirrhosis. *Metab Brain Dis* 28(2):217–220.
42. Butz M, May ES, Häussinger D, Schnitzler A (2013) The slowed brain: Cortical oscillatory activity in hepatic encephalopathy. *Arch Biochem Biophys* 536(2):197–203.
43. Sørensen M (2013) Update on cerebral uptake of blood ammonia. *Metab Brain Dis* 28(2):155–159.
44. Weissenborn K, Heidenreich S, Giewekemeyer K, Rückert N, Hecker H (2003) Memory function in early hepatic encephalopathy. *J Hepatol* 39(3):320–325.
45. Brenner M, et al. (2015) Patients with manifest hepatic encephalopathy can reveal impaired thermal perception. *Acta Neurol Scand*, 10.1111/ane.12376.
46. Butz M, et al. (2010) Motor impairment in liver cirrhosis without and with minimal hepatic encephalopathy. *Acta Neurol Scand* 122(1):27–35.
47. Leke R, et al. (2012) Impairment of the organization of locomotor and exploratory behaviors in bile duct-ligated rats. *PLoS ONE* 7(5):e36322.
48. Magen I, et al. (2009) Cannabidiol ameliorates cognitive and motor impairments in mice with bile duct ligation. *J Hepatol* 51(3):528–534.
49. Cauli O, Llansola M, Erceg S, Felipo V (2006) Hypolocomotion in rats with chronic liver failure is due to increased glutamate and activation of metabotropic glutamate receptors in substantia nigra. *J Hepatol* 45(5):654–661.
50. Sergeeva OA, et al. (2005) Deficits in cortico-striatal synaptic plasticity and behavioral habituation in rats with portacaval anastomosis. *Neuroscience* 134(4):1091–1098.
51. Butterworth RF (2011) Neuroinflammation in acute liver failure: Mechanisms and novel therapeutic targets. *Neurochem Int* 59(6):830–836.
52. Görg B, Bidmon H-J, Häussinger D (2013) Gene expression profiling in the cerebral cortex of patients with cirrhosis with and without hepatic encephalopathy. *Hepatology* 57(6):2436–2447.
53. Coltart I, Tranah TH, Shawcross DL (2013) Inflammation and hepatic encephalopathy. *Arch Biochem Biophys* 536(2):189–196.
54. Dennis CV, et al. (2014) Microglial proliferation in the brain of chronic alcoholics with hepatic encephalopathy. *Metab Brain Dis* 29(4):1027–1039.
55. Kaiser S, Gerok W, Häussinger D (1988) Ammonia and glutamine metabolism in human liver slices: New aspects on the pathogenesis of hyperammonaemia in chronic liver disease. *Eur J Clin Invest* 18(5):535–542.
56. Matsuno T, Goto I (1992) Glutaminase and glutamine synthetase activities in human cirrhotic liver and hepatocellular carcinoma. *Cancer Res* 52(5):1192–1194.
57. Gebhardt R, Reichen J (1994) Changes in distribution and activity of glutamine synthetase in carbon tetrachloride-induced cirrhosis in the rat: Potential role in hyperammonemia. *Hepatology* 20(3):684–691.
58. Kennan AL (1964) Glutamine synthetase activity in rat liver after portacaval shunt. *Endocrinology* 74:805–806.
59. Girard G, Butterworth RF (1992) Effect of portacaval anastomosis on glutamine synthetase activities in liver, brain, and skeletal muscle. *Dig Dis Sci* 37(7):1121–1126.
60. He Y, et al. (2010) Glutamine synthetase in muscle is required for glutamine production during fasting and extrahepatic ammonia detoxification. *J Biol Chem* 285(13):9516–9524.
61. Hof PR, Young WG, Bloom FL, Belichenko PV, Celio M (2000) *Comparative Cytoarchitectonic Atlas of the C57BL/6 and 129/Sv Mouse Brains* (Elsevier, Amsterdam).